Supplementary Information (SI) for Journal of Materials Chemistry B.

SI Appendix:

Supplementary Table 1: Primers used for qRT-RCR

Target	Forward primer（5'-3'）	Reverse primer（5'-3'）
Gapdh	AGTGCCAGCCTCGTCTCATA	GAGAAGGCAGCCCTGGT
Runx2	CAGTTCCTAACGGGCACCAT	AACTTAGGGTCTCGGAGGGAAGG
Spp1	CCAAGCGTGGAAACACACAGCC	GGCTTTGGAACTCGCCTGACTG
Alpl	TATGTCTGGAACCGCACTGAAC	CACTAGCAAGAAGAAGCCTTTGG
Bglap	GCCCTGACTGCATTCTGCCTCT	TCACCACCTTACTGCCCTCCTG
Col1a1	GTACATCAGCCCAAACCCCA	CAGGATCGGAACCTTCGCTT
Pparg	CATTTTTCAAGGGTGCCAGT	TAGATGTGGTACGACCGGAG
Cebpa	GGTGGATAAGAACAGCAACGA	TCAACTCCAACACCTTCTGCT
Fabp4	ATTCGGCACGAGTCCTTGAA	GACCAAGTCCCCTTCTACGC

Supplementary Figures and Figure Legends

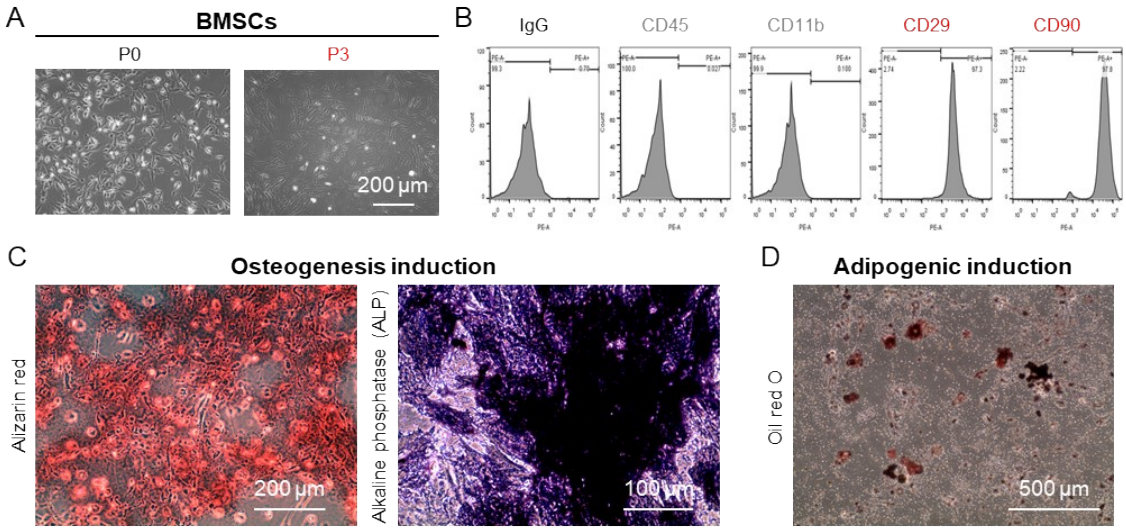

Supplementary Figure 1: Morphological characterization and differentiation potential of isolated rBMSCs

A. Phase contrast microscopy reveals stellate or spindle-shaped at passage 0 (P0) and passage 3 (P3). B. Flow cytometry analysis confirms the rBMSC phenotype, with low expression of CD45 and CD11b, and high expression of CD29 and CD90. C. Alizarin red staining after 14 days of osteogenic induction shows calcified nodule formation. D. ALP staining after 7 days of osteogenic induction demonstrates ALP activity. E. Oil Red O staining after 14 days of adipogenic induction reveals lipid droplet formation.

For osteogenic differentiation, rBMSCs were cultured in osteogenic induction medium (OM) consisting of Dulbecco's Modified Eagle's Medium (DMEM) supplemented with 15% fetal bovine serum (FBS), 100 nM dexamethasone, 5 mM β-glycerophosphate, and 50 μg/ml ascorbic acid. Osteogenic differentiation was assessed by Alizarin Red (Solarbio, China) staining for calcium deposition and alkaline phosphatase (ALP) (Beyotime, China) staining.

For adipogenic differentiation, rBMSCs were cultured in adipogenic induction medium (AM) composed of DMEM supplemented with 10% FBS, 1 μM dexamethasone, 0.5 mM 3-isobutyl-1-methylxanthine, 5 μg/ml insulin, and 500 μM indomethacin. Adipogenic differentiation was assessed by Oil Red O (Solarbio, China) staining for lipid droplet formation.

Characteristics of isolated rBMSCs: The cells exhibited a stellate or spindle shape when cultured in vitro (Supplementary Fig. 1A). Flow cytometry analysis demonstrated low expression of hematopoietic stem cell markers CD45 and CD11b and high expression of MSC markers CD29 and CD90 (Supplementary Fig. 1B), confirming the phenotype of BMSCs. After continuous induction in osteogenic induction medium for 14 days, rBMSCs formed aggregates and stained positively for Alizarin Red, indicating the formation of calcified nodules (Supplementary Fig. 1C). Positive alkaline phosphatase (ALP) staining further confirmed their osteogenic differentiation capability (Supplementary Fig. 1C). Additionally, after treatment with adipogenic induction medium for 14 days, Oil Red O staining revealed intracellular lipid droplet formation, confirming their adipogenic differentiation capability (Supplementary Fig. 1D).

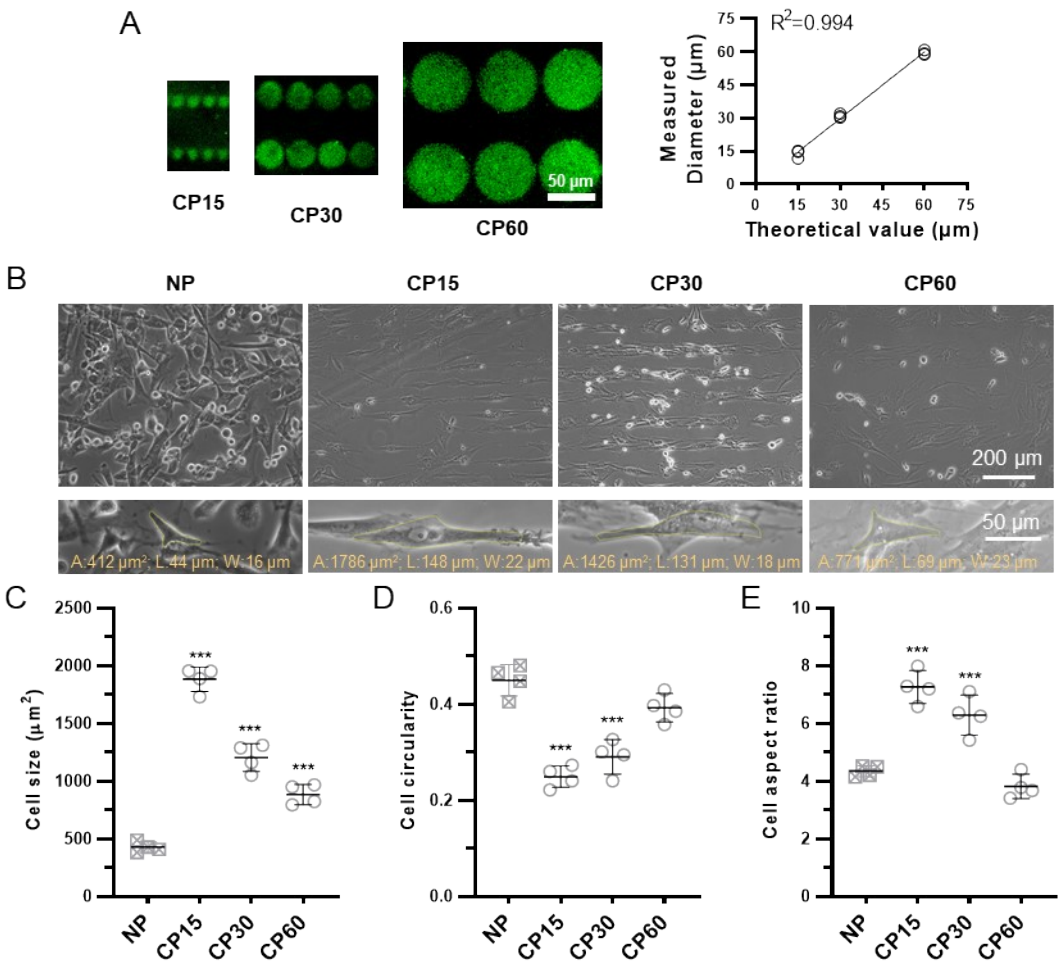

Supplementary Figure 2: Morphology of rBMSCs on circular micropatterned (CP) surfaces. A. Fluorescence microscopy images show Alexa Fluor 488-labeled fibronectin (FN) adsorption on CP surfaces, with quantification of micropattern diameters. B. Cell morphology on CP surfaces at 24 h and a representative cell morphology on each CP surface. C-E: Quantification of rBMSCs morphology, including cell size (C), circularity (D), and aspect ratio (E) on CP surfaces. Mean ± standard deviation (SD); n=4, four independent experiments, with each analyzing six images, and a minimum of 30 cells measured per image. **P＜0.01，***P＜0.001 vs. NP.

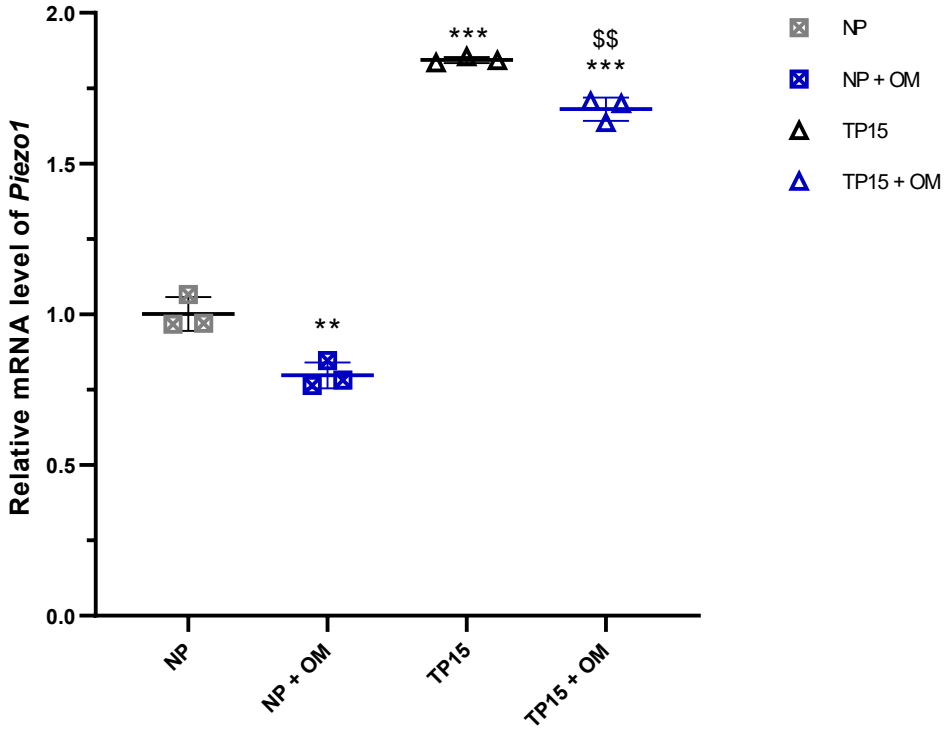

Supplementary Figure 3: Comparision of TP15 surface and OM on Piezo1 expression in rBMSCs. Mean ± standard deviation (SD). n=3. **P<0.01, ***P<0.001 vs. NP; $$P<0.01 vs. TP15.

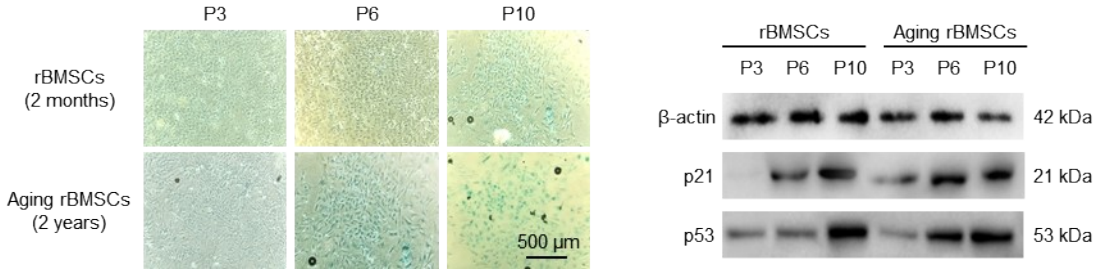

Supplementary Figure 4: Aging rBMSCs isolated from 2 years-old rats. Left: β-galactoglycerase staining; right: western blot detection of p53 and p21.

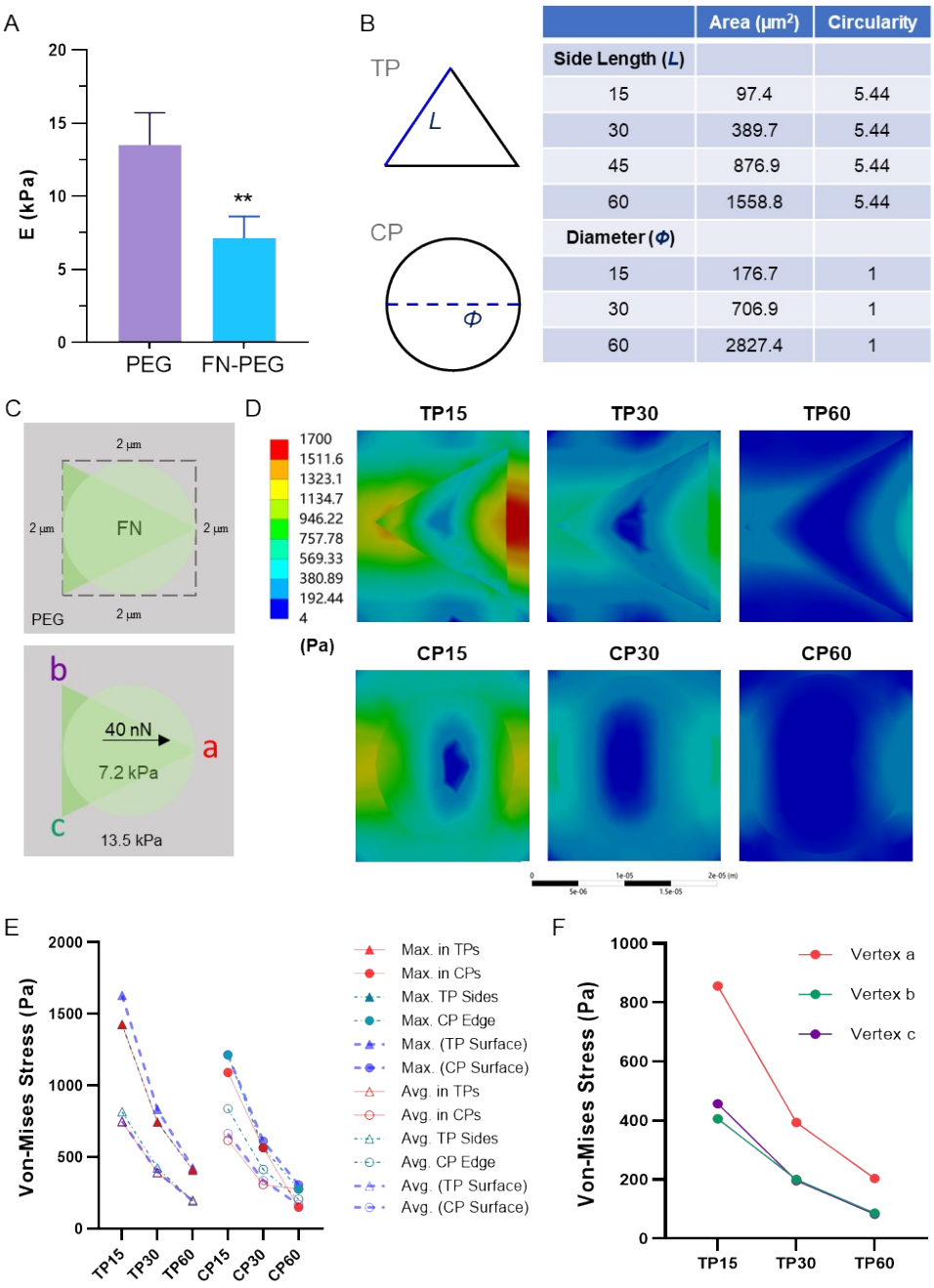

	Area (μm²)	Circularity
Side Length (*L*)		
15	97.4	5.44
30	389.7	5.44
45	876.9	5.44
60	1558.8	5.44
Diameter (*Φ*)		
15	176.7	1
30	706.9	1
60	2827.4	1

Supplemental Figure 5: Mechanical characteristics of micropatterned surfaces. A. Nanoindentation was used to assess the stiffness of micropatterns and the surrounding PEG on the surfaces. **P<0.01. B. Comparison of area and circularity between triangular patterns (TPs) and circular patterns (CPs). C. The numerical computation model with specific parameters. Using the measured stiffness of PEG and fibronectin (FN) coated regions, the stress on TP15 and CP15 surfaces was calculated under a 40 nN force. D. Stress contour illustrating the stress concentration on triangular micropatterns. E. The maximum and average

stress on the micropatterns, entire surfaces, and edges. F. Stress distribution at the three vertices of the TPs.

Stress analysis on Micropatterned Surfaces: The maximum stress on TPs is predominantly concentrated at the edges, with the vertices along the triangular axis exhibiting higher stress than the other two vertices. TP15 demonstrates significantly higher maximum stress on both entire surfaces and edges compared to CPs and other larger TPs, although the average stress on TP surfaces is only slightly higher than that on circular micropatterns (Supplementary Fig. 4). These findings suggest that the concentrated stress on micropatterned surfaces might trigger cellular mechanical responses, leading to morphological changes and lineage commitment.